Histone propionylation is a mark of active chromatin

Adam F Kebede^{1,2}, Anna Nieborak³, Lara Zorro Shahidian³, Stephanie Le Gras¹, Florian Richter^{2,4}, Diana Aguilar Gómez^{3,5}, Marijke P Baltissen⁶, Gergo Meszaros^{1,7,8}, Helena de Fatima Magliarelli¹, Aaron Taudt^{9,10}, Raphael Margueron¹¹, Maria Colomé-Tatché^{9,10,12}, Romeo Ricci^{1,7,8}, Sylvain Daujat¹, Michiel Vermeulen⁶, Gerhard Mittler² & Robert Schneider^{1,3,13}

Histones are highly covalently modified, but the functions of many of these modifications remain unknown. In particular, it is unclear how histone marks are coupled to cellular metabolism and how this coupling affects chromatin architecture. We identified histone H3 Lys14 (H3K14) as a site of propionylation and butyrylation *in vivo* and carried out the first systematic characterization of histone propionylation. We found that H3K14pr and H3K14bu are deposited by histone acetyltransferases, are preferentially enriched at promoters of active genes and are recognized by acylation-state-specific reader proteins. In agreement with these findings, propionyl-CoA was able to stimulate transcription in an *in vitro* transcription system. Notably, genome-wide H3 acylation profiles were redefined following changes to the metabolic state, and deletion of the metabolic enzyme propionyl-CoA carboxylase altered global histone propionylation levels. We propose that histone propionylation, acetylation and butyrylation may act in combination to promote high transcriptional output and to couple cellular metabolism with chromatin structure and function.

Histones are modified by a variety of post-translational modifications (PTMs) that cooperate to regulate chromatin structure and function¹. These PTMs are implicated in the regulation of gene expression, higher-order chromatin structure and response to external stimuli²⁻⁴. Although histone acetylation and methylation are relatively well studied, multiple previously unknown types of histone PTMs have recently been identified¹, but their functions are largely unknown. A subset of these new PTMs comprises lysine acylations, including propionylation (Kpr)⁵, butyrylation (Kbu)⁵, crotonylation (Kcr)⁶, hydoxyisobutyrylation (Khib)⁷, succinylation (Ksuc) and malonylation (Kmal)⁸. Notably, most of these newly discovered histone acylation sites overlap with known histone acetylation (Kac) sites. This observation prompts questions concerning the functional overlap between histone Kac and other short chain acylations⁹.

Among the newly discovered histone acylations, histone lysine propionylation (three-carbon molecule: C3) and butyrylation (C4) were the first reported, and they are, in their chemical structures and properties, most similar to acetylation (C2). Indeed, by adding additional carbon atoms to the lysine side chain, they may be regarded as linear analogs to tetrahedral mono-, di- and tri-methylation^{5,10}. Early reports have suggested that some Kpr and Kbu events may be catalyzed *in vitro* by histone acetyltransferases (HATs), but *in vivo* evidence for this remains lacking¹¹.

The activity of many histone-modifying enzymes is regulated by the intracellular concentrations of metabolites, such as acetyl-CoA, because the metabolites serve as cofactors for the relevant enzyme^{12,13}. Coupling of enzyme activity to cofactor availability has the potential to couple chromatin states to metabolism. Propionyl-CoA, the putative cosubstrate for histone propionylation, originates from oxidation of odd-chain fatty acids and catabolism of branched-chain amino acids. Butyryl-CoA is also an intermediate of fatty acid beta-oxidation¹¹. Thus, histone short chain acylations are potential candidates linking the metabolic state of the cell with chromatin architecture.

We characterized histone H3 lysine propionylation and butyrylation, using site-specific antibodies that we developed. We observed that H3K14 propionylation, as well as butyrylation, were most enriched at the promoters of the most highly expressed genes and, together with acetylation, were able to promote a higher transcriptional output. In agreement with this observation, we found that the most active genes in mouse livers had multiple acylation marks. Notably, inducing changes to the metabolic state in a defined mouse model drove changes in the liver histone acylation profiles. In accordance with acylation states being important for chromatin function, we found that the BAF chromatin-remodeling complex recognizes specific acylation marks. Moreover, using an *in vitro* transcription system, we observed that propionyl-CoA was able to stimulate transcription from a

¹Institut de Génétique et de Biologie Moléculaire et Cellulaire, Illkirch, France. ²Max Planck Institute of Immunobiology and Epigenetics, Freiburg, Germany. ³Institute of Functional Epigenetics, Helmholtz Zentrum München, Neuherberg, Germany. ⁴Goethe-Universität Fachbereich Medizin, Frankfurt, Germany. ⁵Undergraduate Program in Genomic Sciences, National Autonomous University of Mexico, Mexico City, Mexico. ⁶Radboud University Nijmegen, Radboud Institute for Molecular Life Sciences, Nijmegen, the Netherlands. ⁷Université de Strasbourg, Strasbourg, France. ⁸Laboratoire de Biochimie et de Biologie Moléculaire, Nouvel Hôpital Civil, Strasbourg, France. ⁹European Research Institute for the Biology of Ageing, University of Groningen, University Medical Center Groningen, Groningen, the Netherlands. ¹⁰Institute of Computational Biology, Helmholtz Zentrum München, Neuherberg, Germany. ¹¹Institut Curie, Paris, France. ¹²Technical University Munich, Freising, Germany. ¹³Ludwig-Maximilains-Universität München, Faculty of Biology, Munich, Germany. Correspondence should be addressed to R.S. (robert.schneider@helmholtz-muenchen.de).

Received 14 February; accepted 22 September; published online 23 October 2017; doi:10.1038/nsmb.3490

chromatinized template. Taken together, our results suggest that H3K14 propionylation is a previously unknown metabolite-directed histone PTM that defines the transcriptionally active chromatin state.

RESULTS

Identification of histone H3K14 propionylation and butyrylation

To study the functions of Kpr and Kbu in histones, we first aimed to identify which lysines were modified *in vivo*. For this, we performed mass spectrometry analysis of HeLa histones and identified a total of five Kpr and seven Kbu sites on the tails of histones H3 and H4 (**Fig. 1a** and **Supplementary Fig. 1a–d**). Notably, all of the identified sites are also known sites of acetylation (Kac)¹⁴ (**Fig. 1a**).

As models to study histone Kpr and Kbu, we chose to focus on H3K14, because acetylation at H3K14 has been linked with transcriptional activation¹⁴. To study H3K14pr and H3K14bu in vivo, we attempted to raise specific antibodies. After affinity purification, we obtained antibodies specific for both acylations. In peptide dot blot assays, the H3K14pr and H3K14bu antibodies recognized the corresponding immunizing peptides with high specificity (Fig. 1b,c). The antibodies specifically recognized histone H3 in immunoblots (Supplementary Fig. 2a), and signals were competed away by the corresponding immunizing peptides (Supplementary Fig. 2b,c). Next we performed a limited trypsin digestion of native nucleosomes, which removes the histone tails while leaving the DNA-protected core regions largely intact, followed by immunoblotting. We observed a loss of signal for H3K14pr and H3K14bu, as well as for other tail modifications (Fig. 1d), confirming that these antibodies indeed recognize H3 tail modifications. To rule out cross-reactivity with other potential H3 tail acylation sites, we performed additional peptide dot blots on a collection of peptides carrying acetylation, propionylation and butyrylation at major N-terminal lysines of histone H3 (K9, K18, K23 and K27). We did not detect recognition of these modifications (Supplementary Fig. 2d,e). Together, these results strongly suggest that our antibodies were indeed specific for H3K14pr and H3K14bu.

Notably, we also observed an enhanced signal in H3K14pr and H3K14bu when cells were treated with sodium butyrate (NaBu), an inhibitor of class I and class II histone deacetylases¹⁵ (HDACs; **Supplementary Fig. 2a**). However, the precise removal mechanisms of these modifications remain unknown.

We next confirmed the presence of H3K14pr and H3K14bu in different human and mouse cell lines, as well as in a variety of mouse tissues, including liver, kidney and testis (**Supplementary Fig. 2f,g**). In immunofluorescence, H3K14bu also demonstrated a uniform, nuclear dotted pattern that was excluded from DAPI-dense heterochromatic regions and nucleoli (**Supplementary Fig. 2h**), and was reminiscent of active histone marks^{4,16,17}.

HATs propionylate and butyrylate histones

Previous studies performed *in vitro* reported that some HATs, mainly p300 and CBP, also possess propionyltransferase and butyryltransferase activities^{5,18–21}. Indeed, our *in vitro* histone acylation assays using radiolabeled acyl-CoAs revealed the general histone propionylation and butyrylation activity of not only p300 but also the GNAT family HATs, GCN5 and PCAF (**Fig. 2a**). Moreover, these histone acylation assays showed that both GNAT family enzymes are capable of propionylating and butyrylating histone H3 at K14, in addition to their known acetylation activity (**Supplementary Fig. 3a**). This activity is consistent with findings from a previous report showing *in vitro* specificity of PCAF for H3K14 in peptide acylation assays²¹. To demonstrate the enzyme-dependent accumulation of Kpr, we performed a time course *in vitro* acylation assay on histone octamers

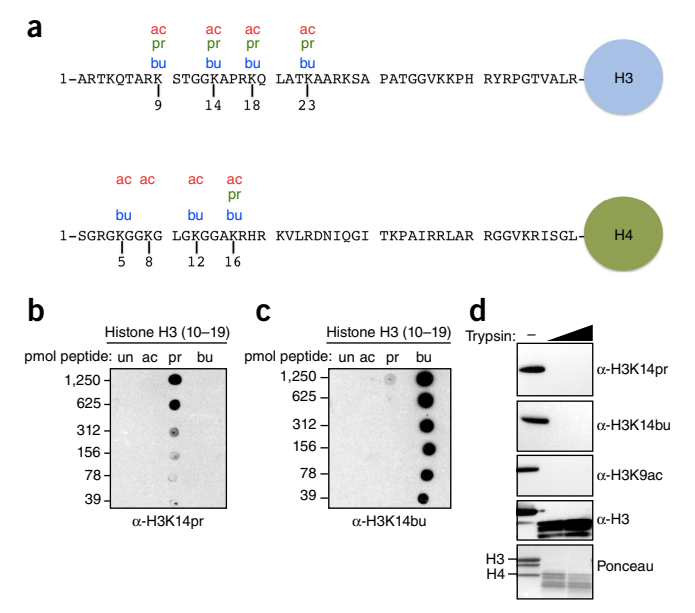


Figure 1 Histone lysine propionylation and butyrylation sites. (a) The N-terminal sequence of histones H3 and H4 with propionylation (pr, green) and butyrylation (bu, blue) sites identified by mass spectrometry in HeLa cells in this study (details and spectra in Supplementary Fig. 1). Known acetylation sites in the N-terminal tails are also shown (ac, red). (b,c) Specificity of anti-H3K14pr (b) and anti-H3K14bu (c) antibodies. Dot blot assays with the indicated affinity-purified antibodies and serial dilutions of H3 (aa10-19) peptides that were unmodified (un), acetylated (ac), propionylated (pr) or butyrylated (bu) at lysine 14. Details of peptide sequences and antibodies used in this study are available in **Supplementary Tables 1** and **2**). (d) Detection of full-length and trypsin-digested nucleosomes with anti-H3K14pr, anti-H3K14bu, anti-H3K9ac and anti-H3 antibodies. Mononucleosomes from HeLa cells were incubated with no (-) or increasing amounts of trypsin to cleave the histone tails and immunoblotted as indicated for H3K14pr, H3K14bu, H3K9ac and H3. Ponceau staining shows full-length histones and the trypsin-digestion products.

and observed a gradual increase in H3K14pr signal only in the presence of GCN5 (**Supplementary Fig. 3b,c**). These results suggest that histone propionylation and butyrylation are, under these conditions, enzyme catalyzed.

To identify which enzymes regulate propionylation and butyrylation of H3K14 *in vivo*, we used a candidate approach based on our *in vitro* data. We used small interfering RNA (siRNA) to deplete GCN5, PCAF, p300 and CBP in cells. Immunoblot analysis revealed that the combined knockdown of *GCN5* (also known as *KAT2A*) and *PCAF* (also known as *KAT2B*) in HeLa cells led to a substantial (~40%) reduction in H3K14pr, but not H3K14bu, levels (**Fig. 2b** and **Supplementary Fig. 3d,f,i**). The reduction in H3K14pr was comparable to that of H3K9ac, a known target of GCN5 and PCAF activity (**Fig. 2b** and **Supplementary Fig. 3f**)²². Following *p300* (official symbol *EP300*) and *CBP* (official symbol *CREBBP*) double knockdown in HeLa cells, we observed a smaller effect (~20% reduction) on the global levels of H3K14pr and H3K14bu (**Fig. 2c** and **Supplementary Fig. 3e,g,h**).

To investigate the effects of GCN5 and PCAF on H3K14pr levels on specific genomic regions, we performed chromatin immunoprecipitation followed by quantitative PCR (ChIP–qPCR) at selected target promoter regions following siRNA-mediated knockdown of both enzymes (**Supplementary Fig. 3j,k**). As expected, we observed reduced enrichment of H3K9ac when both GCN5 and PCAF were depleted at all active

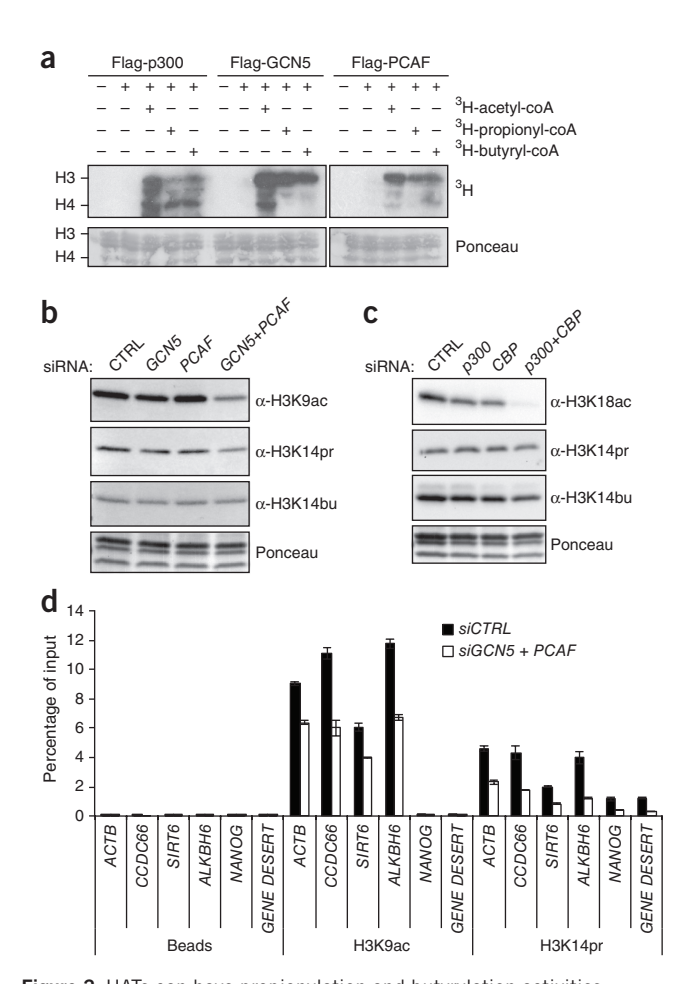


Figure 2 HATs can have propionylation and butyrylation activities. (a) In vitro HAT assays performed with calf thymus histones as substrate and tritium (3H)-labeled acetyl-, propionyl- or butyryl-CoA as acyl donors. Autoradiogram is shown with Ponceau staining as loading control. (b) Immunoblotting for H3K9ac, H3K14pr and H3K14bu following siRNA knockdown of GCN5 and/or PCAF in HeLa cells. A representative experiment of three independent experiments is shown. Uncropped blot images are shown in Supplementary Data Set 1. (c) Immunoblotting for H3K18ac, H3K14pr and H3K14bu following siRNA knockdown of p300 and/or CBP in HeLa cells. (d) ChIP-qPCR analysis of H3K9ac and H3K14pr enrichments in HeLa cells transiently transfected with control siRNA (siCTRL) or siRNAs targeting both GCN5 and PCAF (siGCN5 + PCAF). Mean percentage of input is shown, and error bars indicate s.d. of three technical replicates. Primers for the indicated genes were all near TSSs. 'Gene desert' is a control region on chromosome 2 (Supplementary Table 3).

target promoters (*B-ACTIN* (also known as *ACTB*), *CCDC66*, *SIRT6* and *ALKBH6*) tested²³ (**Fig. 2d**). Notably, enrichment of H3K14pr was also decreased at all of the active gene promoters that we tested, indicating that GCN5 and PCAF indeed contribute to H3K14pr at promoter regions. Taken together, these findings suggest that HATs have acyltransferase activity both *in vitro* and *in vivo*.

Histone propionylation is regulated by a metabolic enzyme

Propionyl-CoA and butyryl-CoA, the putative cosubstrates of Kpr and Kbu, respectively, are intermediates in fatty acid catabolism¹¹ (Fig. 3a). Thus, changes in their levels as a result of metabolic activity may affect levels of histone propionylation and butyrylation, thereby linking cellular metabolism to chromatin acylation states. It is conceivable

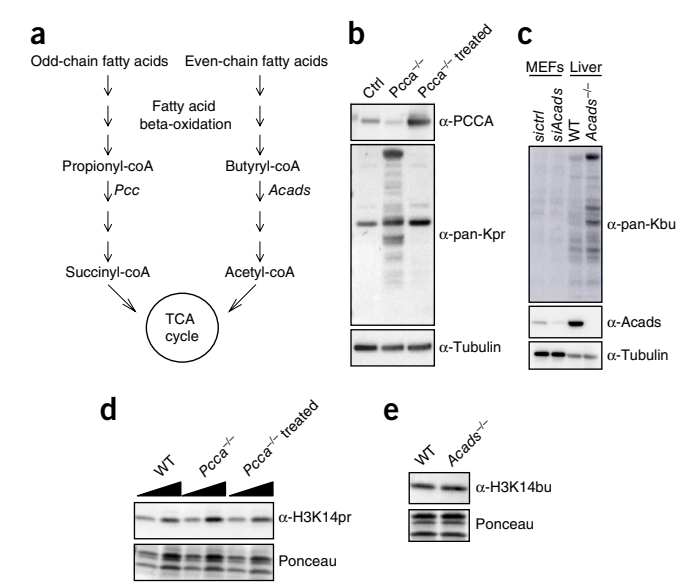


Figure 3 Histone propionylation is sensitive to propionyl-CoA metabolism. (a) Metabolic pathways producing and consuming propionyl-CoA and butyryl-CoA. Both can be derived from fatty acid beta-oxidation. Propionyl-CoA is an end product of odd-chain fatty acid oxidation and can be carboxylated by the PCC complex. Butyryl-CoA is an intermediate in the oxidation of even-chain fatty acids that is further broken down into acetyl-CoA, with the first step being catalyzed by ACADS. (b) Immunoblotting with anti-pan-propionyllysine (pan-Kpr) and anti-PCCA antibodies on lysates prepared from livers of wild type (WT), propionyl-CoA carboxylase alpha subunit-deficient (Pcca-/-) and gene-therapy-treated (Pcca-/-) treated) mice in which PCCA had been reintroduced. Note that, Pcca-/mice show a strong increase in propionyl-CoA levels $^{26}. \ \mbox{Tubulin}$ is a loading control. (c) Immunoblotting with anti-pan-butyryllysine (pan-Kbu) and anti-ACADS antibodies, using whole cell or tissue lysates from either mouse embryonic fibroblasts (MEFs) or livers. ACADS was depleted by siRNA (in MEFs, siAcads) or knocked out (in liver, Acads-/-). Immunoblotting with an antibody to tubulin was used as a loading control. Acads $^{-\!/-}$ livers have elevated butyryl-CoA levels^{24,25}. (d) Immunoblotting with antibody to H3K14pr on acid extracts prepared from livers of WT, Pcca-/- and Pcca-/ $treated^{26}$ mice (quantification in **Supplementary Fig. 3I**). A representative experiment of three independent livers is shown. Uncropped blot images are shown in Supplementary Data Set 1. (e) Immunoblot using an antibody to H3K14bu on acid extracts prepared from WT and Acads-/- mouse livers (quantification in Supplementary Fig. 3m). Ponceau staining is shown as a loading control d and e.

that differential acylation activity could be a result of the cellular concentrations of acetyl-, propionyl- and butyryl-CoA. Previous studies have shown that acetyl-, propionyl- and butyryl-CoA are found at an approximate ratio of 4:2:1 in mouse livers, and this ratio can change following mutations in metabolic enzymes^{24,25}.

We next explored a potential link between H3K14 propionylation and/or butyrylation and metabolic pathways and focused on two candidate enzymes, propionyl-CoA carboxylase (PCC) and acyl-CoA dehydrogenase short-chain (ACADS), both of which degrade their respective CoAs (**Fig. 3a**). Depletion of PCC and ACADS can lead to a global increase in propionyl-CoA and butyryl-CoA concentrations^{24,25}, respectively, and a consequent increase in general protein propionylation and butyrylation (**Fig. 3b,c**). Notably, histones isolated from livers of *Pcca* (alpha subunit of PCC)²⁶ knockout mice displayed higher levels of H3K14pr (~1.3 fold) than H3 from livers of control mice (**Fig. 3d** and **Supplementary Fig. 3l**), as well as a strong increase in general protein propionylation, as detected by pan-specific

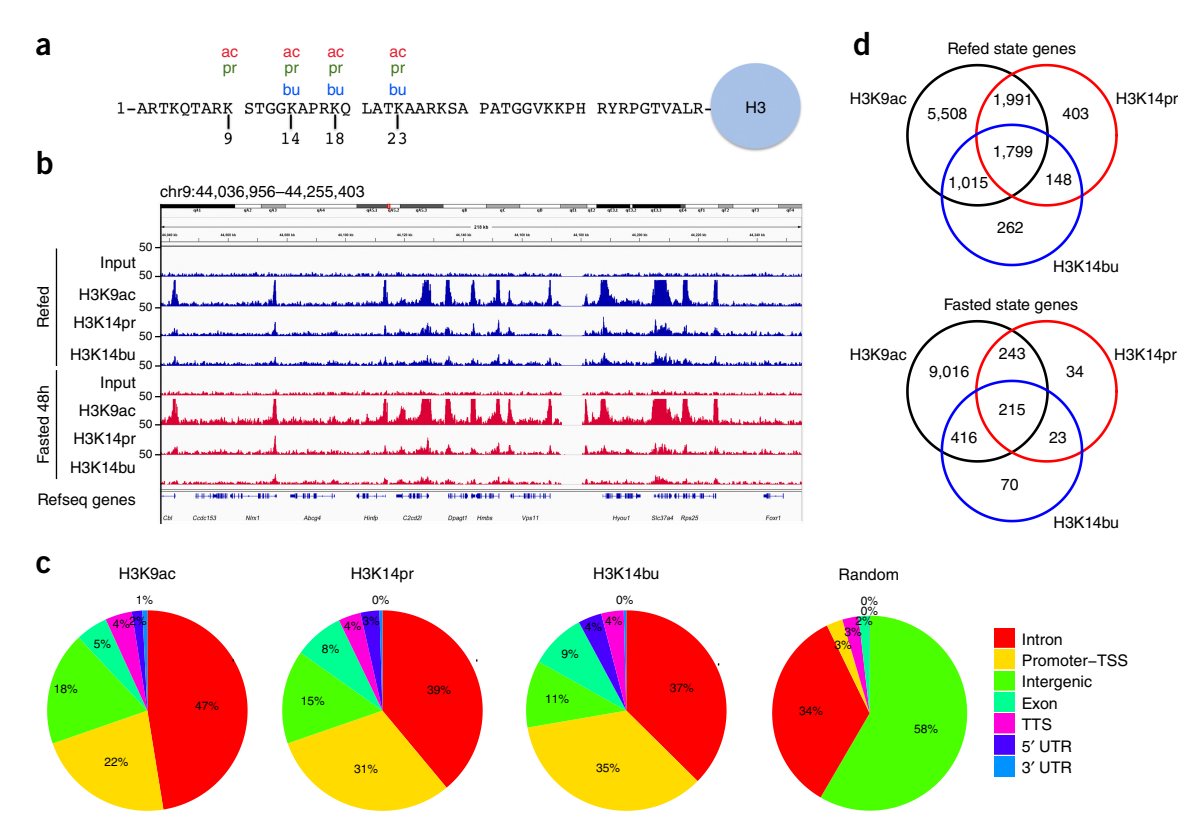


Figure 4 Histone acylations are specifically enriched at active promoter regions. (a) A scheme depicting histone H3 with the acetylation (ac, red), propionylation (pr, green) and butyrylation (bu, blue) sites identified by mass spectrometry in the N-terminal tail of H3 from mouse liver tissue (details and spectra in Supplementary Fig. 4). (b) Genome-browser snapshot of mouse chromosome 9, showing depth-normalized ChIP-seq tracks for Input, H3K9ac, H3K14pr and H3K14bu from livers of mice refed or fasted 48 h. (c) Genomic annotation of H3K9ac, H3K14pr and H3K14bu peaks. (d) Venn diagrams showing overlap between histone-acylation-enriched genes in livers from refed (left) and 48 h fasted (right) mice.

anti-Kpr (**Fig. 3b**). In agreement with this finding, levels of H3K14pr and of general propionylation in livers of *Pcca* knockout mice reverted to wild-type levels when human PCCA was expressed in knockout mice in a gene therapy model²⁶ (**Fig. 3b,d** and **Supplementary Fig. 3l**). Notably, we found that H3K14bu levels remained largely unchanged in livers from *Acads* knockout mice despite increased CoA levels and an increase in general protein butyrylation²⁵ (**Fig. 3c,e** and **Supplementary Fig. 3m**).

Genomic localization of H3K14pr and H3K14bu in the mouse liver

We next addressed the genome-wide distribution of histone Kpr and Kbu. Given that our hypothesis was that histone Kpr and Kbu might be metabolically regulated, we aimed to carry out chromatin immunoprecipitation sequencing (ChIP-seq) experiments in a metabolically relevant tissue, the liver, where we could challenge mice by fasting. First, we confirmed by mass spectrometric analysis of acid-extracted histones that H3K14pr and H3K14bu were present in mouse liver (Fig. 4a and Supplementary Fig. 4). We also found that, in H3, Lys9, Lys18 and Lys23 were propionylated and/or butyrylated in mouse livers (Fig. 4a and data not shown). Next, we performed ChIP-seq experiments using chromatin isolated from livers of mice experiencing different metabolic challenges: either refed (mice fasted for 12 h and fed again for 4 h) or fasted for 48 h. In addition, we performed ChIP-seq to determine the distribution of histone acetylation so that we could compare it to the distribution of butyrylation and propionylation. However, all of the antibodies to H3K14ac that we tested cross-reacted with other H3K14 acylation states (data not shown). Thus, we chose H3K9ac as the prototypical example of a histone acetylation site linked to active genomic region. Previous studies have shown that genomewide profiles of H3K9ac and H3K14ac extensively overlap²⁷.

H3K14pr and H3K14bu displayed overall profiles reminiscent of those of other 'active' histone marks (**Fig. 4b,c**), such as H3K9ac and H3K4me3 (ref. 28). Annotation of H3K14pr- and H3K14bu-enriched regions revealed that they were highly enriched at promoter and transcription start site (TSS) regions (defined as –1 kb to +100 bp), where ~30–35% of the H3K14pr and H3K14bu peaks mapped, as compared with 22% of H3K9ac peaks (**Fig. 4c**). Notably, in livers from refed mice, 87% of both H3K14pr (3,790 of 4,341) and H3K14bu (2,814 of 3,224) marked genes were also enriched for H3K9ac (**Fig. 4d**). Similarly, in livers from fasted mice, we found that 89% (458 of 515) of H3K14pr targets and 87% (631 of 724) of H3K14bu targets were enriched for H3K9ac (**Fig. 4d**). We found that this high degree of overlap was also conserved when we compared our data with recently published²⁹ H3K4me3 data from livers of mice fed *ad libitum* or fasted (**Supplementary Fig. 5a**).

Considering that H3K9ac, H3K14pr and H3K14bu overlapped extensively genome wide (**Fig. 4b–d**), we performed immunoprecipitation experiments with mononucleosomes purified from HeLa cells to test whether these marks could indeed co-occur in the same nucleosomes. We found that H3K14pr or H3K14bu nucleosomes were enriched for H3K9ac and H3K4me3 (**Supplementary Fig. 5b**). In agreement with this result, our mass spectrometric analysis of HeLa histones revealed H3K9ac on the same peptides together with H3K14pr or H3K14bu (**Supplementary Fig. 1c,d**). We conclude that histone acylations can co-occur on chromatin. Despite the high

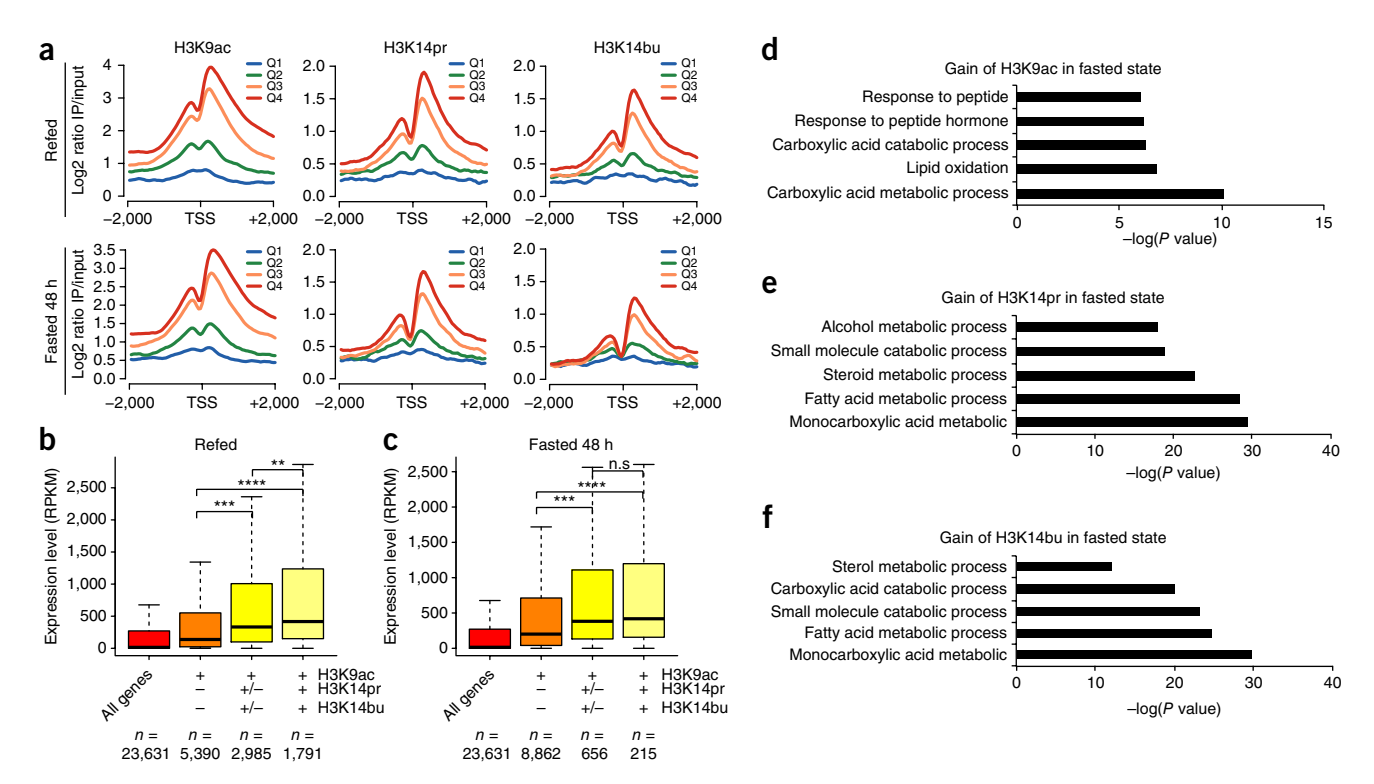


Figure 5 Correlation between histone acylations and gene expression. (a) Input-normalized histone acylation profiles ± 2 kb from the TSSs of genes grouped into four quartiles on the basis of level of expression (obtained from RNA-seq data): Q1, least expressed genes; Q2 and Q3, intermediately expressed genes; Q4, highly expressed genes. IP, immunoprecipitate. (b) Expression levels in reads per kilobase pair per million mapped reads (RPKM) of genes that are enriched in the indicated histone acylation mark(s) ± 1 kb around their TSSs in livers from refed mice. '+' indicates the presence of a mark, and '-' indicates its absence. '+/-' is used to indicate that either H3K14pr or H3K14bu is present, but not both. P values were calculated using the Wilcoxon rank sum test (two-tailed); **P = 1.42×10^{-7} , ***P = 7.93×10^{-79} ; ****P = 4.25×10^{-100} . (c) Expression levels of genes that are enriched in the indicated histone acylation mark(s) ± 1 kb around their TSSs in livers from fasted mice. ***P = 4.08×10^{-20} ; ****P = 1.31×10^{-10} ; not significant. The number of genes plotted is indicated. For box plots in P and P and P the center line is the median, and the central rectangle spans the first quartile (Q1) to the third quartile (Q3) (IQR, interquartile range). The upper whisker extends from the hinge to the largest value no further than P 1.5× IQR from the hinge (Q3 + P 1.5× IQR). The lower whisker extends from the hinge to the smallest value at most P 1.5× IQR of the hinge (Q1 – P 1.5× IQR). Outliers are not shown on the plots. (P 1.50 Gene Ontology biological-process terms associated with a gain of H3K9ac (P 1.5× IQR) in livers from fasted mice, determined with GREAT³³.

overlap between H3K14pr, H3K14bu and H3K9ac target genes, we still found some genes (~11–13%) in which we detected only H3K14pr or H3K14bu enrichments above our threshold (**Fig. 4d**). Gene ontology analysis of such genes from the refed state revealed that these genes may be associated with several important biological processes (**Supplementary Fig. 5c,d**).

H3K14pr and H3K14bu are associated with transcriptionally active chromatin

To gain insight into the roles of histone propionylation and butyrylation in gene expression, we performed RNA-seq, using RNA isolated from mouse livers under the same two metabolic states as described above (that is, refed and 48 h fasted). We observed the same metabolically induced changes in gene expression as those published previously (data not shown)^29. In livers from both refed and fasted mice, we found enrichment of H3K14pr and H3K14bu across TSSs that correlated with RNA expression levels (Fig. 5a), thus suggesting that the enrichments are indicative of efficient gene expression. This result was also consistent with recent reports of enrichment of other histone acylations, such as histone crotonylation (Kcr) and β -hydroxybutyrylation (Kbhb), at active genes 6,30 . Moreover, a comparison of our data with published data for H3K4me3 (ref. 29), H3K9bhb^29 and RNA polymerase II (ser5p)^31 revealed a strong positive correlation (Supplementary Fig. 5e).

Next, we examined the links between gene expression and the cooccurrence of different acylations in more detail. The most active genes in both the refed and the fasted conditions displayed enrichments above threshold of multiple acylations (H3K9ac, H3K14pr and/or H3K14bu) within 1 kb of their TSS (**Fig. 5b,c**). In contrast, genes for which we detected enrichment of only one acylation (that is, H3K9ac) above threshold showed lower expression levels (**Fig. 5b,c**). We analyzed whether 'triple-acylated' genes were associated with specific biological processes and found that, in both the refed and fasted states, 'transcription' and 'covalent chromatin modification' were among the top ten significantly enriched terms (**Supplementary Fig. 5f,g**).

To evaluate the changes in histone acylation between the refed and fasted states, we called differentially enriched peaks using chromstaR³². We found 812, 6,496 and 6,180 differentially enriched regions that were gained in livers of fasted mice for H3K9ac, H3K14pr and H3K14bu, respectively (data not shown). Notably, gene ontology analysis of these regions³³ revealed 'carboxylic acid metabolic process' as the most significantly enriched term (**Fig. 5d–f**). Moreover, other terms related to fatty acid or lipid metabolism were also enriched, thus indicating that lipid metabolism may be a primary target of fasting-induced histone acylations (**Fig. 5d–f**).

Taken together, our data suggest that histone Kpr and Kbu are linked to transcriptional activation. Moreover, in combination with histone acetylation, Kpr and Kbu have a strong predictive power of

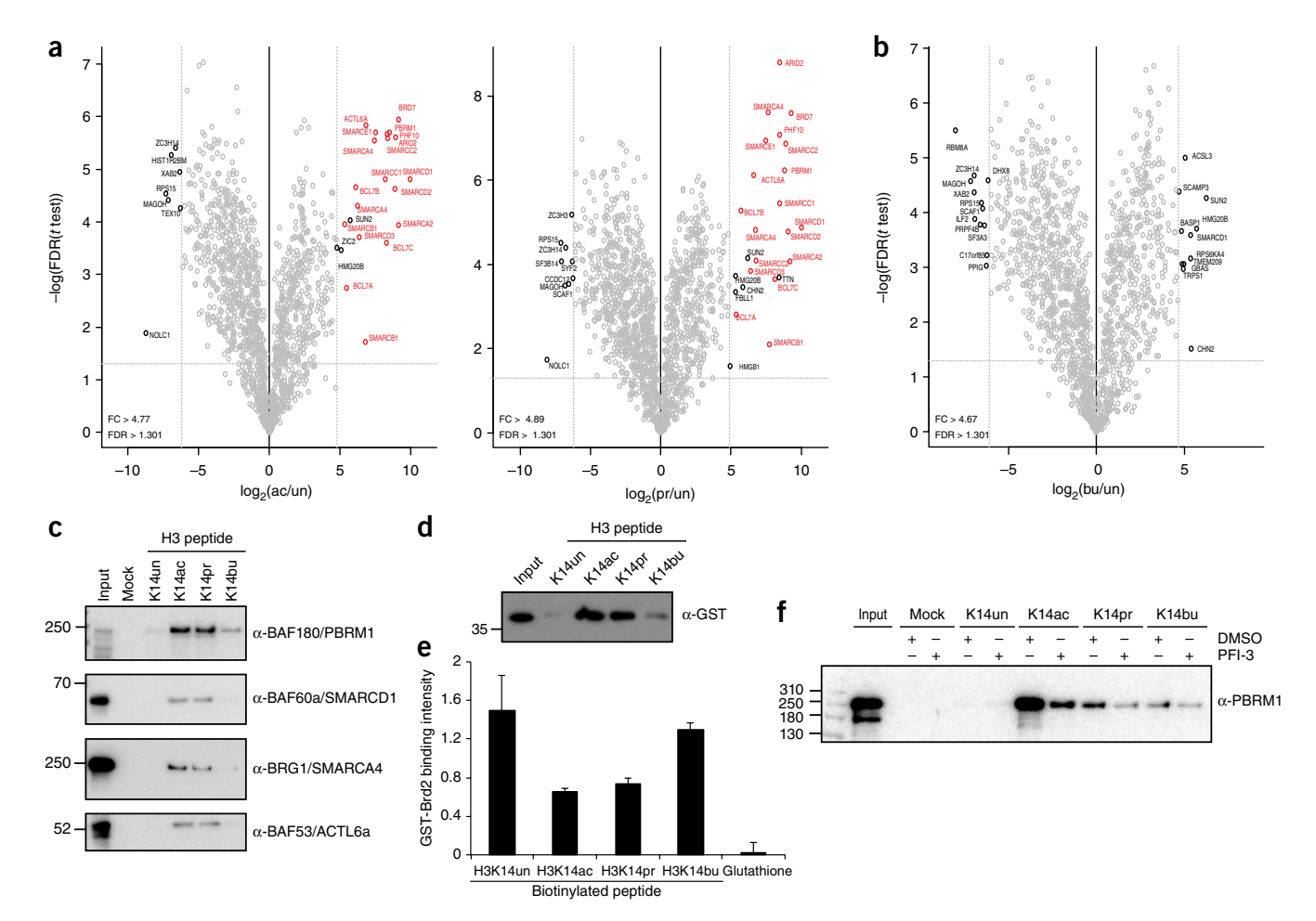


Figure 6 Histone acylations differentially bind the BAF remodeling complex. (a) Volcano plot showing all enriched proteins in H3K14ac (left) and H3K14pr (right) peptide affinity purifications relative to H3K14 unmodified peptides. Proteins beyond the cutoff ($-\log_2$ false discovery rate >1.301) were considered enriched or depleted. Subunits of the (P)BAF complex are in red. (b) Volcano plot showing all enriched proteins in H3K14bu peptide affinity purifications relative to H3K14 unmodified peptide. (c) H3K14 peptide affinity purifications from HeLa nuclear extract, immunoblotted with antibodies against (P)BAF complex subunits (BAF180, BAF60A, BRG1 and BAF53). A representative of two experiments is shown. Uncropped blot images are shown in **Supplementary Data Set 1**. (d) Peptide affinity purifications with GST-tagged bromodomain 2 of BAF180 (PBRM1) (GST-PBRM1(2)). (e) Holdup assay³⁶ with GST-PBRM(2), using biotinylated peptide resins or glutathione beads as a positive control. Unbound protein passed through the filter, and concentrations were measured by capillary electrophoresis. Mean binding intensity is shown, with error bars representing s.d. of three independent assays. (f) H3K14 peptide affinity purification from HeLa nuclear extract incubated in the presence of either DMSO (control) or bromodomain inhibitor PFI-3, and subsequent immunoblotting with antibody to PBRM1.

gene expression levels, and the gain of H3K14pr and H3K14bu in livers of fasted mice targets primarily lipid metabolism pathways.

Histone acylations are differentially bound by the BAF or PBAF remodeling complex

Acetylated lysines can be specifically recognized by bromodomains^{34,35}. However, very little is known about which domains, if any, specifically bind to other short-chain acylations. A previous study¹⁰ found that the recombinant bromodomains of BRD4 bind weakly to propionylated lysines, but an unbiased approach toward identifying binders has not been performed.

Because we observed a correlation between the enrichment of multiple acylations and high levels of gene expression (**Fig. 5b,c**), we explored whether proteins or protein complexes binding to multiple acylation states might be involved in integrating and mediating the effect of acylations on chromatin function. To identify potential binders to histone Kpr and Kbu in an unbiased approach, we performed peptide pulldown experiments followed by mass spectrometry. We found

that H3K14ac and H3K14pr peptides bound a near-identical set of proteins (Fig. 6a and Supplementary Fig. 6a). Notably, prominent among the H3K14ac and H3K14pr binders were all the subunits of the mammalian BAF or PBAF (polybromo-associated BAF) (also known as SWI/SNF) complex. However, we did not detect any BAF or PBAF subunits that bound specifically to H3K14bu (Fig. 6a,b and Supplementary Fig. 6a). We validated these results by immunoblotting for a subset of the (P)BAF subunits (Fig. 6c). Given that the (P)BAF subunits BAF180 (also known as PBRM1), SMARCA4 (BRG1), SMARCA2 (BRM) and BRD7 contain bromodomains, we reasoned that they might be involved in the observed binding activity. To test this possibility, we first asked whether the PBRM1 bromodomain binds acylated H3K14. Indeed, a recombinant second bromodomain of PBRM1 fused to GST (GST-PBRM1(2)) bound directly to peptides containing H3K14pr and H3K14ac (Fig. 6d and Supplementary Fig. 6b). We also validated our result, using an independent holdup assay developed previously³⁶, in which biotinylated peptide resins were used to 'hold up' GST-PBRM1(2) molecules before

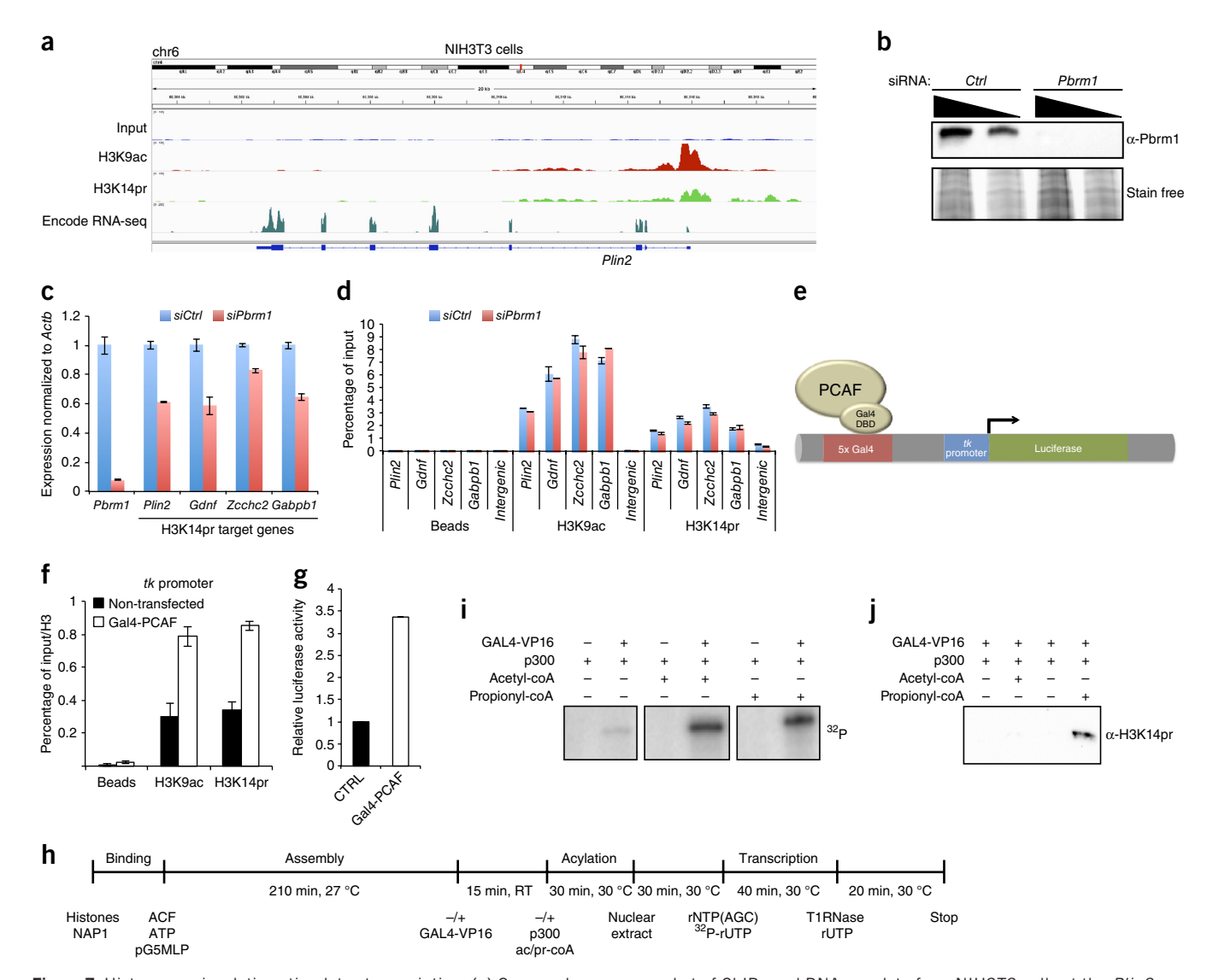


Figure 7 Histone propionylation stimulates transcription. (a) Genome-browser snapshot of ChIP– and RNA-seq data from NIH3T3 cells at the *Plin2* gene. (b) Immunoblot using antibody to Pbrm1 to verify depletion of Pbrm1 after siRNA-mediated knockdown. Stain-free image is shown as loading control. (c) RT–qPCR after knockdown of *Pbrm1* in NIH3T3 cells at selected H3K14pr-enriched genes. Mean expression is normalized to that of β-actin (*Actb*). Error bars represent s.d. of three technical replicates of one representative experiment out of three independent experiments. (d) ChIP–qPCR analysis of H3K9ac and H3K14pr enrichments at the TSSs of the same genes as in c after knockdown of *Pbrm1*. The intergenic region is used as a negative control. The mean percentage of input is shown, and error bars represent s.d. of three technical replicates of a representative experiment out of two experiments. (e) Scheme of the stably integrated reporter system in 293 T-Rex cells. The luciferase gene was under the control of a *TK* promoter downstream of five Gal4-binding sites. PCAF was fused to the Gal4 DNA-binding domain (DBD) to activate transcription of the reporter. (f) ChIP–qPCR analysis of H3K9ac and H3K14pr at the *TK* promoter of the 293 T-Rex cells after transient transfection with or without a plasmid encoding Gal4-PCAF. Error bars represent s.d. of three technical replicates of one representative experiment out of three. Enrichments were normalized to H3. (g) Mean relative luciferase expression after transient transfection of 293 T-Rex cells with a control (CTRL) or *Gal4-PCAF* plasmids. Error bars represent s.d. of three technical replicates of one representative experiment out of three. (h) Scheme of an *in vitro* transcription assay. (i) *In vitro* transcription assay using a chromatin template. The recovered RNA was analyzed with denaturing PAGE, and a representative autoradiogram of two independent experiments is shown. Panels are from the same experiment and same gel. Uncropped autoradiogram is shown in **Supple**

the filtrate was analyzed by capillary electrophoresis. Similarly to the results of the peptide pulldown experiments, H3K14ac and H3K14pr peptides bound GST-PBRM(2), whereas the H3K14un and H3K14bu peptides did not (**Fig. 6e**).

Next, we inhibited BRG1 and PBRM1 bromodomain function in HeLa nuclear extract by using the inhibitor PFI-3, which binds the bromodomains, thus preventing binding to cognate targets³⁷. PFI-3 treatment resulted in a reduction in PBRM1 binding to all H3K14

peptides (**Fig. 6f**). In conclusion, our unbiased approach suggested that Kpr and Kac are recognized by a highly overlapping set of bromodomain containing proteins, including the BAF or PBAF complex. In contrast, the same complexes did not seem to recognize Kbu, presumably because of its longer acyl chain, which in turn might be recognized by yet-unidentified binders.

Because Pbrm1 was a strong candidate binder for H3K14pr in cells, we investigated whether depletion of Pbrm1 affects the expression

of H3K14pr-marked genes. We chose four H3K14pr-target genes and assessed the effect of Pbrm1 knockdown (**Fig. 7a,b**). Notably, in NIH3T3 cells, all of the target genes tested had reduced expression in siPbrm1 cells (**Fig. 7c**). ChIP-qPCR experiments at the TSSs of the same target genes revealed that the enrichment of neither H3K9ac nor H3K14pr was affected (**Fig. 7d**).

Histone propionylation stimulates transcription

To further investigate the role of histone propionylation in transcriptional activation, we applied a stably integrated reporter system in 293 T-Rex cells in which the luciferase gene was under the control of a TK promoter preceded by five Gal4-binding sites (**Fig. 7e**)³⁸. ChIP-qPCR experiments revealed that, following transient transfection of a plasmid driving the expression of PCAF fused to a Gal4 DNA-binding domain, H3K14pr enrichments at the TK promoter increased by ~2.5-fold (**Fig. 7f**). This increase was accompanied by a ~3.3-fold increase in luciferase expression (**Fig. 7g**), thus suggesting that the increased histone acylation at the TK promoter contributed to transcriptional activation.

To test whether propionylation can indeed stimulate transcription, we used a cell-free *in vitro* transcription system in which we could add either acetyl-CoA or propionyl-CoA (**Fig. 7h**). In this system, transcription from chromatinized templates occurs in an activator- and CoA-dependent manner³⁹. Notably, we observed that propionyl-CoA was able to stimulate transcription to a similar extent as acetyl-CoA (**Fig. 7i**). Using our antibody to H3K14pr, we confirmed that H3K14 was indeed propionylated on the *in vitro*-assembled chromatin (**Fig. 7j**). Taken together, our results strongly suggest that histone propionylation stimulates transcription, at least *in vitro*, and does so to a similar extent as one of the hallmarks of transcriptional activation, histone acetylation.

DISCUSSION

Our findings provide an initial functional characterization of histone H3 tail acylations, particularly propionylation at H3K14 and its link to cellular metabolism. Our data integrate histone propionylation into the growing number of non-acetyl histone acylations^{9,40}, and our combined *in vivo* and *in vitro* data suggest a functional role of histone propionylation in transcription.

We found that the HATs p300, GCN5 and PCAF are able to utilize propionyl- and/or butyryl-CoA as acyl-group donors *in vitro*. This activity is consistent with findings from previous studies reporting that p300 and GCN5 propionylate and butyrylate histones *in vitro*^{5,19,21}. However, our results demonstrate that GCN5 and PCAF regulate the levels of histone propionylation (Kpr) *in vivo*. Nevertheless, we cannot exclude the possibility that Kpr and Kbu might also be catalyzed by yet-uncharacterized acyltransferases and may even partially result from nonenzymatic acylation.

Our results identify a previously unknown modification, H3K14 propionylation, *in vivo*. We mapped the enrichment profile of H3K14pr in mouse livers and found that H3K14pr marks active TSSs and promoters. Notably, H3K14pr enrichment levels are strongly correlated with transcriptional activity in two different metabolic states. Our genome-wide analyses predicted that this short-chain acylation functions combinatorially with Kac and Kbu to promote a higher transcriptional output. How nonacetyl histone acylations would support this increased transcription is an intriguing question. Beyond to charge neutralization of the target lysine to potentially increase DNA accessibility, our results suggest that one possible mechanism may be the recruitment of acylation-state-specific binding complexes, as shown previously for histone acetylation^{3,41,42} and

methylation. Notably, different histone lysine methylation states (for example, mono-, di- and trimethylation) lead to the recruitment of distinct readers^{42–44}. In agreement with this result, we found in our unbiased search for binders that the (P)BAF chromatin-remodeling complex⁴⁵⁻⁴⁷ recognizes distinct acylation marks. Thus, high local concentrations of Kac and Kpr might serve to efficiently recruit an overlapping set of transcriptional regulators necessary for high-level transcriptional output. Because we did not identify H3K14bu-specific binders, it is possible that the main function of Kbu might be to deter such binding, for example, preventing (P)BAF complex recruitment and therefore contributing to a dynamic association of factors with chromatin and high transcriptional activity⁴⁸. Alternatively, Kbu may recruit additional binding proteins that we were unable to identify using our approach. Given that no histone H3 tail acetylation (including H3K14) has been associated with effects on global chromatin compaction to date, we do not anticipate any effect of H3K14pr or H3K14bu on global chromatin compaction⁴⁹.

Finally, our demonstration that propionyl-CoA carboxylase, an enzyme involved in metabolic disease^{26,50}, alters global histone propionylation emphasizes a direct link between metabolic pathways that consume the cosubstrates and histone propionylation. Our results also suggest a potential role for histone propionylation in metabolic signaling and disease. Whether the changes observed in global levels of H3K14pr result from alterations in the enrichment of this modification at specific genomic loci remains to be determined.

In conclusion, our study sheds light on the complexity of the regulation of chromatin function by histone modifications through the identification and characterization of previously unknown modification sites and types. Our results demonstrate a role of histone propionylation in transcription and suggest that histone propionylation, in combination with acetylation and butyrylation, may couple cellular metabolic state to chromatin structure and function.

METHODS

Methods, including statements of data availability and any associated accession codes and references, are available in the online version of the paper.

Note: Any Supplementary Information and Source Data files are available in the online version of the paper.

ACKNOWLEDGMENTS

We thank K. Bloom and M. Bennett (Children's Hospital Philadelphia) for Acads knockout tissues; A. Guenzel and M. Barry (Mayo Clinic) for Pcca knockout and gene-therapy-treated tissues; L. Arrigoni and J. Pospisilik for help with liver chromatin preparation; L. Tora (Institut de Genetique et de Biologie Moleculaire et Cellulaire, IGBMC) for baculoviruses expressing GCN5 and PCAF and for anti-GCN5 antibody; P. Laurette and I. Davidson (IGBMC) for antibodies against (P)BAF complex subunits; P. Eberling for peptide synthesis; S. Knapp (University of Frankfurt) for PFI-3 inhibitor; D. Widmann for initial analyses of data; and members of the Schneider laboratory for helpful discussions and reagents. M.C.-T. acknowledges support from the Helmholtz Association's Initiative and Networking Fund and from the University of Groningen (Rosalind Franklin Fellowship). Work by G. Meszaros and R.R. was supported by a European Research Council (ERC) starting grant (ERC-2011-StG, 281271-STRESSMETABOL). Work in the Schneider laboratory was supported by the Agence Nationale de Recherche (CoreAc), the DFG through SFB 1064, the Epigenomics of Common Diseases EpiTrio project and the Helmholtz Gesellschaft. Sequencing was performed by the IGBMC Microarray and Sequencing platform, a member of the 'France Génomique' consortium (ANR-10-INBS-0009).

AUTHOR CONTRIBUTIONS

A.F.K. and R.S. conceived the project. A.F.K. characterized antibodies, performed most of the ChIP, knockdown and peptide pulldown experiments and analyzed data. A.N. contributed to antibody characterization and knockdown experiments, and performed

GAL4 recruitment ChIP and luciferase assays. L.Z.S. performed *in vitro* transcription experiments with the help of R.M. S.L.G. and D.A.G. performed analyses of ChIP and RNA-seq data. F.R. and G. Mittler performed and analyzed histone-modification mass spectrometry experiments. M.P.B. and M.V. performed and analyzed peptide-pulldown mass spectrometry experiments. G. Meszaros, H.F.M. and R.R. contributed to animal fasting and liver cross-linking experiments. A.T. and M.C.-T. performed ChIP-seq data analyses. A.F.K., S.D. and R.S. wrote the manuscript.

COMPETING FINANCIAL INTERESTS

The authors declare no competing financial interests.

Reprints and permissions information is available online at http://www.nature.com/reprints/index.html. Publisher's note: Springer Nature remains neutral with regard to jurisdictional claims in published maps and institutional affiliations.

- Huang, H., Sabari, B.R., Garcia, B.A., Allis, C.D. & Zhao, Y. SnapShot: histone modifications. Cell 159, 458–458.e1 (2014).
- Hanover, J.A., Krause, M.W. & Love, D.C. Bittersweet memories: linking metabolism to epigenetics through O-GlcNAcylation. Nat. Rev. Mol. Cell Biol 13, 312–321 (2012).
- Bannister, A.J. & Kouzarides, T. Regulation of chromatin by histone modifications. Cell Res. 21, 381–395 (2011).
- Kouzarides, T. Chromatin modifications and their function. Cell 128, 693–705 (2007).
- Chen, Y. et al. Lysine propionylation and butyrylation are novel post-translational modifications in histones. Mol. Cell. Proteomics 6, 812–819 (2007).
- Tan, M. et al. Identification of 67 histone marks and histone lysine crotonylation as a new type of histone modification. Cell 146, 1016–1028 (2011).
- Dai, L. et al. Lysine 2-hydroxyisobutyrylation is a widely distributed active histone mark. Nat. Chem. Biol. 10, 365–370 (2014).
- Xie, Z. et al. Lysine succinylation and lysine malonylation in histones. Mol. Cell. Proteomics 11, 100–107 (2012).
- Rousseaux, S. & Khochbin, S. Histone acylation beyond acetylation: terra incognita in chromatin biology. Cell J. 17, 1–6 (2015).
- Vollmuth, F. & Geyer, M. Interaction of propionylated and butyrylated histone H3 lysine marks with Brd4 bromodomains. *Angew. Chem. Int. Edn Engl.* 49, 6768–6772 (2010).
- 11. Lin, H., Su, X. & He, B. Protein lysine acylation and cysteine succination by intermediates of energy metabolism. *ACS Chem. Biol.* **7**, 947–960 (2012).
- Kaelin, W.G. Jr. & McKnight, S.L. Influence of metabolism on epigenetics and disease. Cell 153, 56–69 (2013).
- 13. Wellen, K.E. *et al.* ATP-citrate lyase links cellular metabolism to histone acetylation. *Science* **324**, 1076–1080 (2009).
- Roth, S.Y., Denu, J.M. & Allis, C.D. Histone acetyltransferases. *Annu. Rev. Biochem.* 70, 81–120 (2001).
- Candido, E.P., Reeves, R. & Davie, J.R. Sodium butyrate inhibits histone deacetylation in cultured cells. *Cell* 14, 105–113 (1978).
- Strahl, B.D. & Allis, C.D. The language of covalent histone modifications. *Nature* 403, 41–45 (2000).
- Zhou, V.W., Goren, A. & Bernstein, B.E. Charting histone modifications and the functional organization of mammalian genomes. *Nat. Rev. Genet.* 12, 7–18 (2011).
- 18. Kaczmarska, Z. et al. Structure of p300 in complex with acyl-CoA variants. Nat. Chem. Biol. 13, 21–29 (2017).
- 19. Ringel, A.E. & Wolberger, C. Structural basis for acyl-group discrimination by human Gcn5L2. *Acta Crystallogr. D Struct. Biol.* **72**, 841–848 (2016).
- Albaugh, B.N., Arnold, K.M. & Denu, J.M. KAT(ching) metabolism by the tail: insight into the links between lysine acetyltransferases and metabolism. *ChemBioChem* 12, 290–298 (2011).
- Leemhuis, H., Packman, L.C., Nightingale, K.P. & Hollfelder, F. The human histone acetyltransferase P/CAF is a promiscuous histone propionyltransferase. *ChemBioChem* 9, 499–503 (2008).
- Jin, Q. et al. Distinct roles of GCN5/PCAF-mediated H3K9ac and CBP/p300-mediated H3K18/27ac in nuclear receptor transactivation. EMBO J. 30, 249–262 (2011).
- Bonnet, J. et al. The SAGA coactivator complex acts on the whole transcribed genome and is required for RNA polymerase II transcription. Genes Dev. 28, 1999–2012 (2014).

- Pougovkina, O., Te Brinke, H., Wanders, R.J.A., Houten, S.M. & de Boer, V.C. Aberrant protein acylation is a common observation in inborn errors of acyl-CoA metabolism. *J. Inherit. Metab. Dis.* 37, 709–714 (2014).
- Palladino, A.A., Chen, J., Kallish, S., Stanley, C.A. & Bennett, M.J. Measurement of tissue acyl-CoAs using flow-injection tandem mass spectrometry: acyl-CoA profiles in short-chain fatty acid oxidation defects. *Mol. Genet. Metab.* 107, 679–683 (2012).
- Guenzel, A.J. et al. Generation of a hypomorphic model of propionic acidemia amenable to gene therapy testing. Mol. Ther. 21, 1316–1323 (2013).
- Karmodiya, K., Krebs, A.R., Oulad-Abdelghani, M., Kimura, H. & Tora, L. H3K9 and H3K14 acetylation co-occur at many gene regulatory elements, while H3K14ac marks a subset of inactive inducible promoters in mouse embryonic stem cells. BMC Genomics 13, 424 (2012).
- 28. Shen, Y. *et al.* A map of the *cis*-regulatory sequences in the mouse genome. *Nature* **488**, 116–120 (2012).
- Xie, Z. et al. Metabolic regulation of gene expression by histone lysine βhydroxybutyrylation. Mol. Cell 62, 194–206 (2016).
- Sabari, B.R. et al. Intracellular crotonyl-CoA stimulates transcription through p300catalyzed histone crotonylation. Mol. Cell 58, 203–215 (2015).
- Koike, N. et al. Transcriptional architecture and chromatin landscape of the core circadian clock in mammals. Science 338, 349–354 (2012).
- Taudt, A., Nguyen, M.A., Heinig, M., Johannes, F. & Colome-Tatche, M. chromstaR: Tracking combinatorial chromatin state dynamics in space and time. Preprint at https://www.biorxiv.org/content/early/2016/02/04/038612/ (2016).
- McLean, C.Y. et al. GREAT improves functional interpretation of cis-regulatory regions. Nat. Biotechnol. 28, 495–501 (2010).
- 34. Filippakopoulos, P. et al. Histone recognition and large-scale structural analysis of the human bromodomain family. Cell 149, 214–231 (2012).
- Sanchez, R. & Zhou, M.-M.Therole of human bromodomains in chromatin biology and gene transcription. *Curr. Opin. Drug Discov. Devel.* 12, 659–665 (2009).
- Vincentelli, R. et al. Quantifying domain-ligand affinities and specificities by highthroughput holdup assay. Nat. Methods 12, 787–793 (2015).
- Fedorov, O. et al. Selective targeting of the BRG/PB1 bromodomains impairs embryonic and trophoblast stem cell maintenance. Sci. Adv. 1, e1500723 (2015).
- 38. Sanulli, S. *et al.* Jarid2 methylation via the PRC2 complex regulates H3K27me3 deposition during cell differentiation. *Mol. Cell* **57**, 769–783 (2015).
- An, W., Palhan, V.B., Karymov, M.A., Leuba, S.H. & Roeder, R.G. Selective requirements for histone H3 and H4 N termini in p300-dependent transcriptional activation from chromatin. *Mol. Cell* 9, 811–821 (2002).
- Sabari, B.R., Zhang, D., Allis, C.D. & Zhao, Y. Metabolic regulation of gene expression through histone acylations. *Nat. Rev. Mol. Cell Biol.* 18, 90–101 (2017).
- Struhl, K. Histone acetylation and transcriptional regulatory mechanisms. Genes Dev. 12, 599–606 (1998).
- Taverna, S.D., Li, H., Ruthenburg, A.J., Allis, C.D. & Patel, D.J. How chromatinbinding modules interpret histone modifications: lessons from professional pocket pickers. *Nat. Struct. Mol. Biol.* 14, 1025–1040 (2007).
- Musselman, C.A., Lalonde, M.-E., Côté, J. & Kutateladze, T.G. Perceiving the epigenetic landscape through histone readers. *Nat. Struct. Mol. Biol.* 19, 1218–1227 (2012).
- Jenuwein, T. & Allis, C.D. Translating the histone code. Science 293, 1074–1080 (2001).
- Kadoch, C. et al. Proteomic and bioinformatic analysis of mammalian SWI/SNF complexes identifies extensive roles in human malignancy. Nat. Genet. 45, 592–601 (2013).
- Hargreaves, D.C. & Crabtree, G.R. ATP-dependent chromatin remodeling: genetics, genomics and mechanisms. Cell Res. 396–420 (2011).
- Kasten, M.M., Clapier, C.R. & Cairns, B.R. SnapShot: Chromatin remodeling: SWI/ SNF. Cell 144, 310.e1 (2011).
- Goudarzi, A. et al. Dynamic competing histone H4 K5K8 acetylation and butyrylation are hallmarks of highly active gene promoters. Mol. Cell 62, 169–180 (2016).
- Shogren-Knaak, M. et al. Histone H4-K16 acetylation controls chromatin structure and protein interactions. Science 311, 844–847 (2006).
- 50. Shchelochkov, O.A., Carrillo, N. & Venditti, C. Propionic acidemia. in *GeneReviews* (eds. Pagon, R.A. *et al.*) (Seattle, 1993).

ONLINE METHODS

Rabbit polyclonal-antibody generation and purification. All antibodies used were raised in rabbits (Biogenes GmbH) with the immunizing peptides (synthesized by Biosyntan or in-house facility) STGGK(pr)APRKQGGC, STGGK(bu)APRKQGGC for H3K14pr and H3K14bu, respectively, according to a protocol from Biogenes. A list of peptides used in this study is available in Supplementary Table 1. For purification, immunizing peptides were coupled to Sulfolink beads (Pierce) and used as bait according to the manufacturer's instructions. Different ratios (50:1 to 10:1) of serum to antibody were used depending on the antibody. In some cases, depletion with beads coupled to unmodified or acetylated peptides was applied to obtain non-cross-reacting antibodies. Antibodies were eluted with 0.1 M glycine, pH 2.5, and dialyzed against PBS and stored at 4 or $-20\,^{\circ}\text{C}$.

Peptide dot blots. Peptides were quantified on the basis of lyophilized-pellet weight as well as with the Scopes method (absorbance at 205 nm)⁵¹. To test the specificity of histone-modification antibodies, serial dilutions of chemically synthesized peptides with or without different modifications at different sites (H3K14 or H4K16) were spotted directly onto nitrocellulose membranes of 0.1 μ m pore size. The membrane was air-dried for 30 min and probed with antibodies.

Mass spectrometric identification of histone lysine propionylation and butyrylation. Acid-extracted histones from HeLa cells were separated by C8 reversed-phase chromatography (Vydac C8, 5- μm beads, 300-Å pore size, 200 × 14 mm) on a GE Biosciences SMART system, as previously described⁵². We routinely loaded 400-500 µg of total protein (as estimated by Bradford assay) and collected fractions of 0.3 ml. To reduce the amount of samples for MS analysis two neighboring fractions were pooled, so that all histone fractions contained approximately 20 μg of protein. HeLa histone-protein-containing samples were separated by 4-20% Tris-glycine gels (1 mm, NuPAGE, Invitrogen). Dialyzed acid-extracted histones from mouse liver were separated on a 16% Tris-glycine WedgeWell gel (Invitrogen). Bands were stained with colloidal Coomassie stain (colloidal blue, Invitrogen), and histone bands were excised and digested either by limited trypsin proteoloysis (HeLa and mouse liver histones) or Arg-C (HeLa histones) digestion. Limited trypsin digestion was performed in the following way. After reduction/alkylation with DTT (10 mM in 50 mM ammonium bicarbonate, 56 °C, 45 min) and iodoacetamide (55 mM, 25 °C, 20 min, dark) the gel pieces were subjected to extensive washing cycles and a final dehydration step (acetonitrile incubation followed by vacuum evaporation). After rehydration of the gel pieces with trypsin on ice (Promega, 12.5 ng/µl in 50 mM ammonium bicarbonate) we performed tryptic digestion for 15 min (HeLa histones) or 20 min (mouse liver histones) at 37 °C and stopped proteolysis instantly by acidification (TFA 1% (v/v) final concentration) and peptide desalting. ArgC digestion was performed similarly, but enzyme incubation was carried out overnight. Throughout the procedure, we tried to avoid using alcohols as organic solvents, to minimize formation of artificial post-translational modifications. Peptide samples were desalted on STAGE tips, as described previously⁵³, and analyzed via LC-MS with the following parameters. LC-MS parameters for HeLa histones: samples were separated within 60 min with a linear gradient starting from 4% buffer B (80% MeCN in 0.5% acetic acid) to 60% buffer B at a flow rate of 250 nl/min, and this was followed by a washout step (95% buffer B, 8 min, 500 nl/min) and reequilibration (2% buffer B, 7 min, 500 nl/min). Mass spectrometry (OrbitrapXL+ETD) was performed essentially as previously described⁵² except that we acquired both Top10 CID and ETD data for most of the samples. LC-MS parameters for mouse liver histones: Peptides were separated on a 20-cm (75-μm ID) in-house-packed (ReproSil-Pur C18-AQ, 1.9 μm beads, Dr. Maisch Laboratories) fused silica emitter nanocolumn with a 60-min nonlinear gradient (0-8%, 5 min; 8-45%, 40 min; 45-80%, 4 min; 80%, 5 min; 80-0%, 1 min; 0%, 4.5min) of buffer B (80% MeCN in 0.1% formic acid) at a flow rate of 250 nl/min via an Easy nLC1000 UHPLC interfaced with a Q Exactive mass spectrometer. MS acquisition used a Top10 DDA workflow. MS full scans (50-ms max. IT) were performed at 70,000 resolution (at m/z 200; profile mode) with a scan window of 300 to 1,650 m/z and an AGC target value of 3e⁶. HCD MS/MS scans (120 ms max. IT) were acquired at 35,000 resolution, an AGC target of 1×10^5 and an isolation window of 1.6 AMU (NCE 28, exclusion of charge states +1 and unassigned), Data analysis of HeLa histone samples was conducted in PEAKS Studio 7.5, enabling the 'inchorus' mode (the latter including a Mascot 2.2 database search) and

the Peaks PTM algorithm. We performed PEAKS-studio database searches with the following parameters. Parent-mass error tolerance, 10 p.p.m., fragment-ion error tolerance, 0.5 Da (CID, ETD) and charge-dependent precursor-ion m/z correction for charge sates 1+ to 5+. We allowed a maximum of two missed cleavages for ArgC and up to four missed cleavages for limited trypsin digestion, including peptides with two non-enzyme-specific ends. Carbamidomethylation was set as a fixed modification. As variable modifications, we enabled methionine oxidation; acetylation, propionylation and butyrylation of lysine; methylation and dimethylation of arginine and lysine; and trimethylation of lysine. In addition, we also considered modifications occurring at protein N termini. Data analysis of mouse liver histones was conducted essentially as described above but with PEAKS studio 8.0 with the following changes. The HCD-spectrum fragmention tolerance was set to 0.02 Da, and cleavage specificity was set to fully tryptic (allowing four missed cleavages). MS/MS spectra of peptides carrying PTMs were accepted at an FDR of 1% and subjected to manual curation.

SDS-PAGE, immunoblotting and peptide competition. Either self-casted or 4-20% min-PROTEAN TGX stain-free precast gels (Bio-Rad) were used for SDS-PAGE, and proteins were transferred with a Trans-Blot Turbo transfer system (Bio-Rad) to nitrocellulose membranes, according to the manufacturer's instructions. Membranes were blocked in Tris-buffered saline-Tween (TBST) with 0.2% Tween and 4% BSA at room temperature (RT) for 1 h. Different amounts of antibody were incubated with the membrane in TBST with 4% bovine serum albumin (BSA) and incubated with gentle agitation at 4 °C overnight. For peptide competition experiments, antibodies were pre-incubated with peptides for 30 min at 4 °C before adding membranes. The membranes were washed with three changes of TBST for 5 min each and incubated with a secondary antibody conjugated to horseradish peroxidase (HRP) in TBST with 4% BSA at RT for 1 h. The membrane was washed again with three changes of TBST for 5min before antibody binding was detected by incubation of the membrane with an enhanced chemiluminescent (ECL) HRP substrate (Millipore or Bio-Rad) and imaged using film or ChemiDoc Imaging system (Bio-Rad). Quantifications of western blots were done using the ImageLab software (Bio-Rad) according to instruction manual.

Immunofluorescence. Mouse embryonic fibroblasts (MEFs) were seeded on glass coverslips 1 d before the experiment, so that they were 80-90% confluent by the next day. Coverslips were washed twice with PBS and fixed at RT with 4% paraformaldehyde (PFA) and 2% sucrose in PBS for 10 min. Fixation was stopped by washing coverslips three times with PBS. The cells were permeabilized with 0.5% Triton X-100 in PBS at RT for 20 min, washed two times in PBS and blocked with 4% BSA in PBST (with 0.2% Tween-20) at RT for 1h. Primary antibodies were diluted 1:1,000-2,000 in 4% BSA in PBST, and the coverslips were incubated upside down in 100 µl antibody solution at 4 °C in a wet chamber overnight. The cover slips were washed three times for 5 min each in PBST and then incubated at RT with the fluorophore-coupled secondary antibody diluted 1:200 in 4% BSA in PBST for 45 min. The coverslips were washed again three times for 10 min in PBS and were than mounted on glass slides in Vectashield mounting medium (Vector laboratories) containing the DNA intercalating dye DAPI. The coverslips were sealed with nail varnish and stored at 4 °C in the dark. Imaging was done using Leica SP8 UV confocal microscope.

Cell lines. All cell cultures were maintained at 37 °C in a humidified atmosphere containing 5% $\rm CO_2$. HeLa, human embryonic kidney (HEK293), Raw264.7 macrophages and MCF-7 cells were maintained in Dulbecco's modified Eagle's medium, high glucose (DMEM, PAA), supplemented with 10% fetal bovine serum (PerBio), 1% L-glutamine (200 mM) and 1× Pen/Strep (100×) solution (PAA). For NIH3T3 cells, 10% newborn calf serum (NCS) was used with all other components same as the other cells. Mycoplasma testing was done for HeLa and NIH3T3 cells by an in-house tissue culture facility.

Acid extraction of histones from cells and tissues. For acid extraction, cells were harvested and washed in ice-cold PBS once. The cell pellet was resuspended in PBS containing 0.5% Triton X-100 (v/v), protease inhibitors and 10 mM sodium butyrate (NaBu) at a cell density of $10^7 \mbox{cells/ml}$. The cells were incubated on ice for 10 min to lyse the cell membrane, pelleted and washed again in half of the volume of the same buffer. The nuclear pellet was acid-extracted by resuspension in 0.2 M HCl and incubation on ice by at 4×10^7 cells/ml density for at least

30 min. After acid extraction, the sample was centrifuged at 17,000g for 15 min and the acidic supernatant containing the histones transferred to a new tube. Acid extracts were neutralized with 1/5 volume of 1 M Tris, pH 9.5, and protein concentrations were measured with Bradford assays. Acid extraction of histones from tissues was carried out as described previously⁵⁴. After the 0.4 N $\rm H_2SO_4$ extraction step, supernatants were neutralized with 1/2 volume of 1 M Tris, pH 9.5, and dialyzed against 1× PBS.

Histone acylation assays. Full-length HATs (p300, Flag-GCN5 and Flag-PCAF) were expressed and purified with a baculovirus system, as previously described bifferent histone substrates (calf thymus histones (Sigma (H9250)) or recombinant octamers) were mixed in a final reaction volume of 30 μ l with 1× HAT buffer (5% glycerol, 50 mM Tris, pH 8.0, 0.1 mM EDTA, pH 8.0) containing 10 mM NaBu, 1× Complete protease-inhibitor cocktail (Roche), 1 mM DTT and 40 μ M acyl-CoA (Sigma). For radioactive assays [3 H]acetyl-CoA (specific activity 11.6 Ci/mmol, Hartmann Analytic), [3 H]propionyl-CoA (specific activity 100 Ci/mmol, American Radiolabeled Chemicals) or [3 H]butyryl-CoA (specific activity 110 Ci/mmol, American Radiolabeled Chemicals) were used. Reactions were incubated at 30 °C for 1 h, stopped by addition of 6 μ l of 6× Laemmli buffer and boiling for 5 min at 95 °C and loaded on SDS-PAGE gels. For the acylation dot blot time-course assay, 2 μ l of reaction (300 ng octamers) was spotted at each time point before immunoblotting.

siRNA transfection of mammalian cells. ON-TARGETplus SMARTpool siRNAs were purchased from Dharmacon (GE Healthcare). siRNAs were resuspended to $100\,\mu\text{M}$ stock concentration in $1\times$ siRNA resuspension buffer (Thermo Fischer Scientific) and stored at -20 °C. For transfection, siRNAs were used at 10 nM final concentration to transfect HeLa cells with Lipofectamine RNAiMAX (Invitrogen) transfection reagent. The transfections were carried out with the Forward Transfection protocol provided in the manufacturer's instructions. Cells were harvested 72 h post-transfection for RT–qPCR, chromatin immunoprecipitation (ChIP) and/or western blot analysis. A list of siRNAs used in this study are provided in **Supplementary Table 4**.

RNA isolation and quantitative PCR. Total RNA was isolated with a Zymo Quick RNA prep kit (Zymo) according to the manufacturer's instructions. 300 μ l RNA lysis buffer was used per well of a six-well plate. RNA concentration was measured with a NanoDrop 2000 spectrophotometer (Thermo Fischer Scientific). 0.5–1 μ g total RNA was used for each reverse-transcription reaction. cDNA was synthesized with RevertAid First Strand cDNA Synthesis Kits (Thermo Fischer Scientific) using oligo(dT) primer according to the protocol provided by Thermo. cDNA was diluted 1:2 or 1:5 in Ultra-pure H₂O before RT–qPCR (Light Cycler, Roche).

Animal handling and preparation of chromatin from mouse livers. Mice from the C57BL/6J strain were used for all experiments. Maintenance and fasting experiments were done in accordance with the ethical regulations in the IGBMC and the Institut Clinique de la Souris in Strasbourg (ICS), France in compliance with the French and European legislation on the care and use of laboratory animals. All animal experimentation was approved by the Direction des Services Vétérinaires du Bas-Rhin, Strasbourg, France. Refed control mice were fasted for 12 h during the day (7 a.m. to 7 p.m. followed by a short refeeding (7 p.m. to 11 p.m.)). This procedure was done to synchronize fed mice and as a better control than *ad libitum* mice. Fasted mice were transferred into cages without food for 48 h (10 p.m. to 10 p.m.). The experiments were not randomized and were not performed with blinding.

Mice for ChIP experiments were all 8- to 14-week-old males. The protocol to formaldehyde-cross-link fresh mouse livers was adapted from a previous study 56 with some modifications. All dissection and perfusion steps were done at room temperature. Cross-linking time was measured from the time formaldehyde reached the liver, as calculated on the basis of flow rate and tubing volume. Livers were perfused with 1% formaldehyde in PBS for 5 min. After cross-linking, livers were dissected out and placed in petri dishes containing 5 ml of cold buffer A on ice and diced into small pieces. The pieces were transferred into a 15-ml glass homogenizer (Kontes) and 5 ml more buffer A used to wash any remaining liver pieces. Livers were then homogenized with a type A pestle with $\sim 10-15$ strokes up until there were no clumps remaining. To remove debris, liver homogenate

was filtered stepwise through a 250- μ m tissue strainer (Pierce) into 15-ml conical tube and kept on ice until all livers were processed. Liver homogenate was then either stored at –80 °C after snap freezing in liquid nitrogen or further processing to prepare chromatin.

ChIP. To prepare chromatin, the NEXSON protocol was used as previously described⁵⁷. ChIP was done according to previous protocols^{52,58}. For immunoprecipitation with antibodies against histone acylations an amount of chromatin equivalent to 25 μg DNA was used. Before immunoprecipitation, the chromatin was diluted 1:10 with dilution buffer and precleared with 20-80 µl of a 50% slurry of salmon sperm and BSA-blocked Protein A/Protein G (3:1 mix) Sepharose beads (GE Healthcare) in dilution buffer for 1 h. After the precleared chromatin was recovered by centrifugation, antibody was added for immunoprecipitation overnight. 40 µl of Protein A and Protein G bead mix slurry was used to bind immunocomplexes for 3-4 h at 4 °C. The bound immunocomplexes were collected at 2,000g for 1 min, washed twice with low-salt ChIP buffer (20 mM Tris-HCl, pH 8.0, 2 mM EDTA, 1% Triton X-100, 0.1% SDS and 150 mM NaCl), twice with high-salt ChIP buffer (with 500 mM NaCl) and once with LiCl wash buffer (20 mM Tris-HCl, pH 8, 1 mM EDTA, 250 mM LiCl, 1 mM EDTA, 1% NP-40 and 1% sodium deoxycholate) at 4 °C. After a final wash in TE buffer (10 mM Tris pH 8, and 1 mM EDTA) the beads were resuspended in 200 μ l freshly prepared elution buffer (1% SDS and 0.1 M NaHCO₃), and the immunocomplexes were eluted by incubation at 30 °C in a thermoshaker (Eppendorf) at 900 r.p.m. for 30 min. The eluates were de-cross-linked and purified with a PCR purification kit (Qiagen) before being used for ChIP-seq library preparation or qPCRs. A list of all primers used in this study can be found in Supplementary Table 3.

ChIP-seq data analysis. The ChIP-seq library was prepared according to Illumina protocols, and sequencing was done with the HiSeq2500 (Illumina) platform with a read length of 1× 50 bp. We obtained at least 30 million reads per ChIP-seq sample. Only sequences with base-quality phred scores greater than 30 were used. Sequenced reads were mapped to the reference genome Mouse, mm9, with Bowtie 1 (ref. 59). Bowtie 1.0.0 was run with the following arguments: -m 1—strata--best -y -S -l40 -p 2. fastq --S. SAMtools was used to filter and sort uniquely mapping reads and generate bam files⁶⁰. Bam files were converted to bed files with BEDtools⁶¹. Bam files were converted to bigwigs with *deeptools*⁶² for visualization in a genome browser, IGV⁶³ or UCSC⁶⁴.

MACS1.4 was used for peak calling for H3K9ac under the following parameters: --nomodel,--gsize 1.87e+9 and --qvalue 0.05 (refs. 65,66). For H3K14pr and H3K14bu, peak calling was performed in SICER⁶⁷ with the settings: effective genome size fraction, 0.8; window size 200 bps; gap size, 1,000 bp; redundancy threshold, 1.

To find the overlapping regions between samples, *Operate on Genomic Intervals* in Galaxy⁶⁸ or BEDtools was used, and Venny was used to plot Venn diagrams⁶⁹ after defining target genes as genes with a peak within 1 kb of their transcription start site. Homer⁷⁰ was used to annotate peaks to different genomic regions. A GTF file containing annotations mm9.ensgene.gtf was downloaded from Ensembl (Ensembl v67). Average profiles of histone marks across transcription start sites or peaks were made in seqMINER⁷¹. Gene Ontology analysis was performed with DAVID6.8 (ref. 72) by using Ensembl gene IDs as input.

Differential peaks between the refed and the fasted conditions were called in chromstaR 32 . Replicates were handled by chromstaR internally. Differential regions for every mark between the refed and fasted conditions (chromstaR mode = 'differential') were called with a bin size of 500 bp with a step size of 100 bp. To increase the stringency of the peak calls, differential regions were kept if the maximum posterior probability of the differential state anywhere within the region was higher than $(1-10^{-4})$. Differential regions were exported for GO term enrichment analysis in GREAT 33 . For the gain of bu in the fasted state and the gain of pr in the fasted state, we considered only differential regions with a differential score >0.999999 and >0.9999999, respectively, to reduce the number of differential regions tested.

RNA-seq and data analysis. RNA-seq data were generated from total RNA isolated from three refed and three 48-h-fasted mice and sequenced with the HiSeq2500 (Illumina) platform with 1×50 -bp read length. Reads were mapped onto the mm9 assembly of the mouse genome with TopHat v2.0.10 (ref. 73) and the bowtie2 v2.1.0 aligner⁷⁴. Only uniquely aligned reads were retained for further

analyses. Quantification of gene expression was performed in HTSeq v0.5.4p3 (ref. 75) by using gene annotations from Ensembl release 67. Read counts were normalized across libraries with a method proposed previously 76 . Comparisons of interest were performed with a previously proposed method implemented in the DESeq2 Bioconductor library (DESeq2 v1.0.19) 77 . Resulting P values were adjusted for multiple testing using the Benjamini–Hochberg method 78 . Genes were considered upregulated if the \log_2 fold change was greater than 1 and the adjusted P value was less than 0.05. Genes were considered downregulated if the \log_2 fold change was less than -1 and the adjusted P value was less than 0.05.

Peptide pulldown and identification of binder proteins. Peptide pulldowns using nuclear extracts (prepared according to Dignam protocol 79) were performed with the Vermeulen protocol 80 in three independent experiments with some changes as follows. C-terminally biotinylated peptides were first bound to streptavidin–Sepharose beads (GE) with a five-fold excess of peptide to saturate the binding capacity of the beads. Each pulldown reaction contained $10{\text -}20~\mu\text{l}$ of saturated beads and 500 μg of nuclear extract in a total volume of 600 μl pulldown binding buffer (50 mM Tris-HCl, pH 8, 150 mM NaCl, 0.25% NP-40, 1 mM DTT, 10 sodium butyrate, 10 mM nicotinamide and 1× protease-inhibitor cocktail (Roche)). The pulldown mix was incubated at 4 °C in a rotation wheel. Beads were then washed four times with 1 ml pulldown wash buffer (with 300 mM NaCl) for 5 min on a wheel. Bound proteins were eluted by boiling in 1× Laemmli buffer. In-gel digestion and mass spectrometric identification of bound proteins was performed as previously described 80 . Holdup assays for validation were performed as previously described 80 .

Gal4 recruitment assay. T-Rex 293 cells (Invitrogen) with a stably integrated 5×Gal4RE-tk-luc-neo plasmid driving the expression of firefly luciferase under the control of the *TK* promoter downstream of five Gal4 DNA-binding sites were provided by R.M. and grown according to the manufacturer's instructions. Plasmid encoding PCAF (amino acids 352–832) fused to the Gal4 DNA-binding domain (DBD) or control plasmid pGL3-U6-sgRNA-PGK-puro was cotransfected with pRL-CMVwith Lipofectamine 3000 (Invitrogen). pRL-CMV, a *Renilla* reporter plasmid, was used to normalize firefly luciferase values for transfection efficiency in each well. Firefly and *Renilla* luciferase activities were measured 24 h after transfection with a Dual-Luciferase Reporter Assay System (Promega E1910) or cells cross-linked for chromatin immunoprecipitation.

In vitro transcription assay. Wild-type recombinant histones were expressed in *Escherichia coli* and purified from inclusion bodies as previously described⁸¹. Histone octamers were refolded and assembled with the previously described pG5MLP 5S array⁸² by NAP1 and ACF⁸³. *In vitro* transcription assays were performed in the presence of acetyl-CoA, propionyl-CoA or no coenzyme⁸⁴.

Statistics. The Wilcoxon test was used to evaluate the significance of the differences between median values of box plots. For all quantified western blot and RT–qPCR results, s.d. values of three technical or independent experiments were calculated using Microsoft Excel.

Data availability. A **Life Sciences Reporting Summary** for this paper is available. All ChIP–seq and RNA-seq data are available at the GEO database under superseries accession number GSE101598. All other data are available upon request.

- 51. Scopes, R.K. Measurement of protein by spectrophotometry at 205 nm. *Anal. Biochem.* **59**, 277–282 (1974).
- 52. Tropberger, P. *et al.* Regulation of transcription through acetylation of H3K122 on the lateral surface of the histone octamer. *Cell* **152**, 859–872 (2013).

- Rappsilber, J., Mann, M. & Ishihama, Y. Protocol for micro-purification, enrichment, pre-fractionation and storage of peptides for proteomics using StageTips. *Nat. Protoc.* 2, 1896–1906 (2007).
- Rumbaugh, G. & Miller, C.A. Epigenetic changes in the brain: measuring global histone modifications. *Methods Mol. Biol.* 670, 263–274 (2011).
- 55. Demény, M.A. *et al.* Identification of a small TAF complex and its role in the assembly of TAF-containing complexes. *PLoS One* **2**, e316 (2007).
- Chaya, D. & Zaret, K.S. Sequential chromatin immunoprecipitation from animal tissues. *Methods Enzymol.* 376, 361–372 (2004).
- 57. Arrigoni, L. et al. Standardizing chromatin research: a simple and universal method for ChIP-seq. Nucleic Acids Res. 44, e67 (2016).
- Di Cerbo, V. et al. Acetylation of histone H3 at lysine 64 regulates nucleosome dynamics and facilitates transcription. eLife 3, e01632 (2014).
- Langmead, B., Trapnell, C., Pop, M. & Salzberg, S.L. Ultrafast and memory-efficient alignment of short DNA sequences to the human genome. *Genome Biol.* 10, R25 (2009).
- Li, H. et al. The Sequence Alignment/Map format and SAMtools. Bioinformatics 25, 2078–2079 (2009).
- Quinlan, A.R. & Hall, I.M. BEDTools: a flexible suite of utilities for comparing genomic features. *Bioinformatics* 26, 841–842 (2010).
- Ramírez, F., Dündar, F., Diehl, S., Grüning, B.A. & Manke, T. deepTools: a flexible platform for exploring deep-sequencing data. *Nucleic Acids Res.* 42, W187–W191 (2014).
- Thorvaldsdóttir, H., Robinson, J.T. & Mesirov, J.P. Integrative Genomics Viewer (IGV): high-performance genomics data visualization and exploration. *Brief. Bioinform.* 14, 178–192 (2013).
- 64. Kent, W.J. et al. The human genome browser at UCSC. Genome Res. 12, 996–1006 (2002).
- Zhang, Y. et al. Model-based analysis of ChIP-Seq (MACS). Genome Biol. 9, R137 (2008).
- Feng, J., Liu, T., Qin, B., Zhang, Y. & Liu, X.S. Identifying ChIP-seq enrichment using MACS. *Nat. Protoc.* 7, 1728–1740 (2012).
- 67. Zang, C. *et al.* A clustering approach for identification of enriched domains from histone modification ChIP-Seq data. *Bioinformatics* **25**, 1952–1958 (2009).
- Afgan, E. et al. The Galaxy platform for accessible, reproducible and collaborative biomedical analyses: 2016 update. Nucleic Acids Res. 44 W1, W3–W10 (2016)
- Oliveros, J.C. Venny: an interactive tool for comparing lists with Venn's diagrams. http://bioinfogp.cnb.csic.es/tools/venny/index.html (2007).
- Heinz, S. et al. Simple combinations of lineage-determining transcription factors prime cis-regulatory elements required for macrophage and B cell identities. Mol. Cell 38, 576–589 (2010).
- Ye, T. et al. seqMINER: an integrated ChIP-seq data interpretation platform. Nucleic Acids Res. 39, e35 (2011).
- Huang, W., Sherman, B.T. & Lempicki, R.A. Systematic and integrative analysis of large gene lists using DAVID bioinformatics resources. *Nat. Protoc.* 4, 44–57 (2009).
- Kim, D. et al. TopHat2: accurate alignment of transcriptomes in the presence of insertions, deletions and gene fusions. Genome Biol. 14, R36 (2013).
- Langmead, B. & Salzberg, S.L. Fast gapped-read alignment with Bowtie 2. Nat. Methods 9, 357–359 (2012).
- 75. Anders, S., Pyl, P.T. & Huber, W. HTSeq--a Python framework to work with high-throughput sequencing data. *Bioinformatics* **31**, 166–169 (2015).
- Anders, S. & Huber, W. Differential expression analysis for sequence count data. Genome Biol. 11, R106 (2010).
- 77. Love, M.I., Huber, W. & Anders, S. Moderated estimation of fold change and dispersion for RNA-seq data with DESeq2. *Genome Biol.* **15**, 550 (2014).
- Benjamini, Y. & Hochberg, Y. Controlling the false discovery rate: a practical and powerful approach to multiple testing. J. R. Stat. Soc. Series B Stat. Methodol. 57, 289–300 (1995).
- Dignam, J.D., Lebovitz, R.M. & Roeder, R.G. Accurate transcription initiation by RNA polymerase II in a soluble extract from isolated mammalian nuclei. *Nucleic Acids Res.* 11, 1475–1489 (1983).
- Vermeulen, M. Identifying chromatin readers using a SILAC-based histone peptide pull-down approach. *Methods Enzymol.* 512, 137–160 (2012).
- Luger, K., Rechsteiner, T.J. & Richmond, T.J. Expression and purification of recombinant histones and nucleosome reconstitution. *Methods Mol. Biol.* 119, 1–16 (1999).
- An, W. & Roeder, R.G. Reconstitution and transcriptional analysis of chromatin in vitro. Methods Enzymol. 377, 460–474 (2004).
- Ito, T., Bulger, M., Pazin, M.J., Kobayashi, R. & Kadonaga, J.T. ACF, an ISWIcontaining and ATP-utilizing chromatin assembly and remodeling factor. *Cell* 90, 145–155 (1997).
- Margueron, R. et al. Ezh1 and Ezh2 maintain repressive chromatin through different mechanisms. Mol. Cell 32, 503–518 (2008).

natureresearch

Corresponding author(s)	: Robert Schneider	
Initial submission	Revised version	Final submission

Life Sciences Reporting Summary

Nature Research wishes to improve the reproducibility of the work that we publish. This form is intended for publication with all accepted life science papers and provides structure for consistency and transparency in reporting. Every life science submission will use this form; some list items might not apply to an individual manuscript, but all fields must be completed for clarity.

For further information on the points included in this form, see Reporting Life Sciences Research. For further information on Nature Research policies, including our data availability policy, see Authors & Referees and the Editorial Policy Checklist.

<u> </u>	Experimental design			
1.	Sample size			
	Describe how sample size was determined.	No sample-size calculation was performed.		
2.	Data exclusions			
	Describe any data exclusions.	No data were excluded.		
3.	Replication			
	Describe whether the experimental findings were reliably reproduced.	All findings were reliably reproduced.		
4.	Randomization			
	Describe how samples/organisms/participants were allocated into experimental groups.	Not applicable		
5. Blinding				
	Describe whether the investigators were blinded to group allocation during data collection and/or analysis.	no blinding was done.		
	Note: all studies involving animals and/or human research participants must disclose whether blinding and randomization were used.			
6. Statistical parameters For all figures and tables that use statistical methods, confirm that the following items are present in relevant figure legends (or in the Methods section if additional space is needed).				
		irm that the following items are present in relevant figure legends (or in the		
n/a	Confirmed			
	The exact sample size (n) for each experimental group/condition, given as a discrete number and unit of measurement (animals, litters, cultures, etc.)			
\times	A description of how samples were collected, noting whether measurements were taken from distinct samples or whether the same sample was measured repeatedly			
	A statement indicating how many times each experiment was replicated			
	The statistical test(s) used and whether they are one- or two-sided (note: only common tests should be described solely by name; more complex techniques should be described in the Methods section)			
	A description of any assumptions or corrections, such as an adjustment for multiple comparisons			
	The test results (e.g. <i>P</i> values) given as exact values whenever possible and with confidence intervals noted			
	A clear description of statistics including central tendency (e.g. median, mean) and variation (e.g. standard deviation, interquartile range)			
	Clearly defined error bars			
	See the web collection on statis	stics for biologists for further resources and guidance.		

Software

Policy information about availability of computer code

7. Software

Describe the software used to analyze the data in this study.

No custom algorithims, that are not in published literature, were used. All other details are described in the Online methods section.

For manuscripts utilizing custom algorithms or software that are central to the paper but not yet described in the published literature, software must be made available to editors and reviewers upon request. We strongly encourage code deposition in a community repository (e.g. GitHub). *Nature Methods* guidance for providing algorithms and software for publication provides further information on this topic.

▶ Materials and reagents

Policy information about availability of materials

8. Materials availability

Indicate whether there are restrictions on availability of unique materials or if these materials are only available for distribution by a for-profit company.

all unique materials are available upon request

9. Antibodies

Describe the antibodies used and how they were validated for use in the system under study (i.e. assay and species).

The major antibodies used (anti-H3K14pr and anti-H3K14bu) were validated by peptide dotblots, western blots (both from human and mouse cells), peptide competition assays and/or immunofluorescence. Other antibodies were validated by manufacturer or were kind gifts and in some cases were revalidated using siRNA knockdown in human (e.g anti-p300, anti-GCN5, anti-PCAF) or mouse cells (anti-Acads). Details of all antibodies used is in Supplementary table S2.

10. Eukaryotic cell lines

- a. State the source of each eukaryotic cell line used.
- b. Describe the method of cell line authentication used.
- c. Report whether the cell lines were tested for mycoplasma contamination.
- d. If any of the cell lines used are listed in the database of commonly misidentified cell lines maintained by ICLAC, provide a scientific rationale for their use.

IGBMC tissue culture facility

None of the cell lines were authenticated

Cell lines were not tested for mycoplasma contamination except for HeLa and NIH3T3 cells which were mycoplasma tested by the IGBMC tissue culture facility.

no commonly misidentified cell lines were used

Animals and human research participants

Policy information about studies involving animals; when reporting animal research, follow the ARRIVE guidelines

11. Description of research animals

Provide details on animals and/or animal-derived materials used in the study.

Male mice from C57BL/6J strain aged 8-12 weeks were used for all experiments.

Policy information about studies involving human research participants

12. Description of human research participants

Describe the covariate-relevant population characteristics of the human research participants.

Study did not involve human research participants.